Received: 1 March 2023 | Revised: 19 July 2023 | Accepted: 22 August 2023

DOI: 10.1002/jev2.12364

RESEARCH ARTICLE

Profiling extracellular vesicle surface proteins with 10 μL peripheral plasma within 4 h

Jie He[1,2] | **Hengyu Li**[3] | **John Mai**[4] | **Yuqing Ke**[1,2] | **Chunhui Zhai**[1,2] | **Jiao Jiao Li**[5] | **Lai Jiang**[1,2] | **Guangxia Shen**[1,2] | **Xianting Ding**[1,2]

[1]Department of Anesthesiology and Surgical Intensive Care Unit School of Medicine and School of Biomedical Engineering, Xinhua Hospital, Shanghai Jiao Tong University, Shanghai, China

[2]State Key Laboratory of Oncogenes and Related Genes, Institute for Personalized Medicine, Shanghai Jiao Tong University, Shanghai, China

[3]Department of Breast and Thyroid Surgery, Changhai Hospital, Naval Military Medical University, Shanghai, China

[4]Alfred E. Mann Institute for Biomedical Engineering, University of Southern California, Los Angeles, California, USA

[5]School of Biomedical Engineering Faculty of Engineering and IT, University of Technology Sydney, Sydney, NSW, Australia

Correspondence
Guangxia Shen and Xianting Ding, Department of Anesthesiology and Surgical Intensive Care Unit, Xinhua Hospital, School of Medicine and School of Biomedical Engineering, and State Key Laboratory of Oncogenes and Related Genes, Institute for Personalized Medicine, Shanghai Jiao Tong University, Shanghai, China. Email: gxshen@sjtu.edu.cn; dingxianting@sjtu.edu.cn

Hengyu Li, Department of Breast and Thyroid Surgery, Changhai Hospital, Naval Military Medical University, Shanghai, China.
Email: lhy@smmu.edu.cn

Funding information
Shanghai Municipal Education Commission, Grant/Award Number: 21SG10; National Natural Science Foundation of China, Grant/Award Numbers: 22077079, 31771088, 32071405, 81871448, T2122002; Shanghai Municipal Health Comission, Grant/Award Number: 2019CXJQ03; Shanghai Jiao Tong University, Grant/Award Numbers: 2020 SJTU-HUJI, Agri-X20200101, YG2021ZD19, YG2022QN014, YG2023ZD09; Science and Technology Commission of Shanghai Municipality, Grant/Award Number: 22Z510202478; National Key Research and Development Program of China, Grant/Award Numbers: 2022YFC2601700, 2022YFF0710202

Abstract

Extracellular vesicle (EV) surface proteins, expressed by primary tumours, are important biomarkers for early cancer diagnosis. However, the detection of these EV proteins is complicated by their low abundance and interference from non-EV components in clinical samples. Herein, we present a MEmbrane-Specific Separation and two-step Cascade AmpLificatioN (MESS2CAN) strategy for direct detection of EV surface proteins within 4 h. MESS2CAN utilises novel lipid probes (long chains linked by PEG2K with biotin at one end, and DSPE at the other end) and streptavidin-coated magnetic beads, permitting a 49.6% EV recovery rate within 1 h. A dual amplification strategy with a primer exchange reaction (PER) cascaded by the Cas12a system then allows sensitive detection of the target protein at 10 EV particles per microliter. Using 4 cell lines and 90 clinical test samples, we demonstrate MESS2CAN for analysing HER2, EpCAM and EGFR expression on EVs derived from cells and patient plasma. MESS2CAN reports the desired specificity and sensitivity of EGFR (AUC = 0.98) and of HER2 (AUC = 1) for discriminating between HER2-positive breast cancer, triple-negative breast cancer and healthy donors. MESS2CAN is a pioneering method for highly sensitive in vitro EV diagnostics, applicable to clinical samples with trace amounts of EVs.

KEYWORDS
breast cancer, extracellular vesicles, in vitro diagnostics, protein analysis

1 | INTRODUCTION

Extracellular vesicles (EVs) are collections of nano- and micrometre-sized membrane-enclosed vesicles, which are secreted by cells into body fluids to enable cellular communication (Kilic et al., 2022; van Niel et al., 2022). EVs carry a variety of biomolecules inherited from their parent cells (including nucleic acids, proteins, lipids and metabolites), and are involved in a wide range of physiological and pathological processes (Mathieu et al., 2019). Notably, many tumour-derived EV proteins have been identified

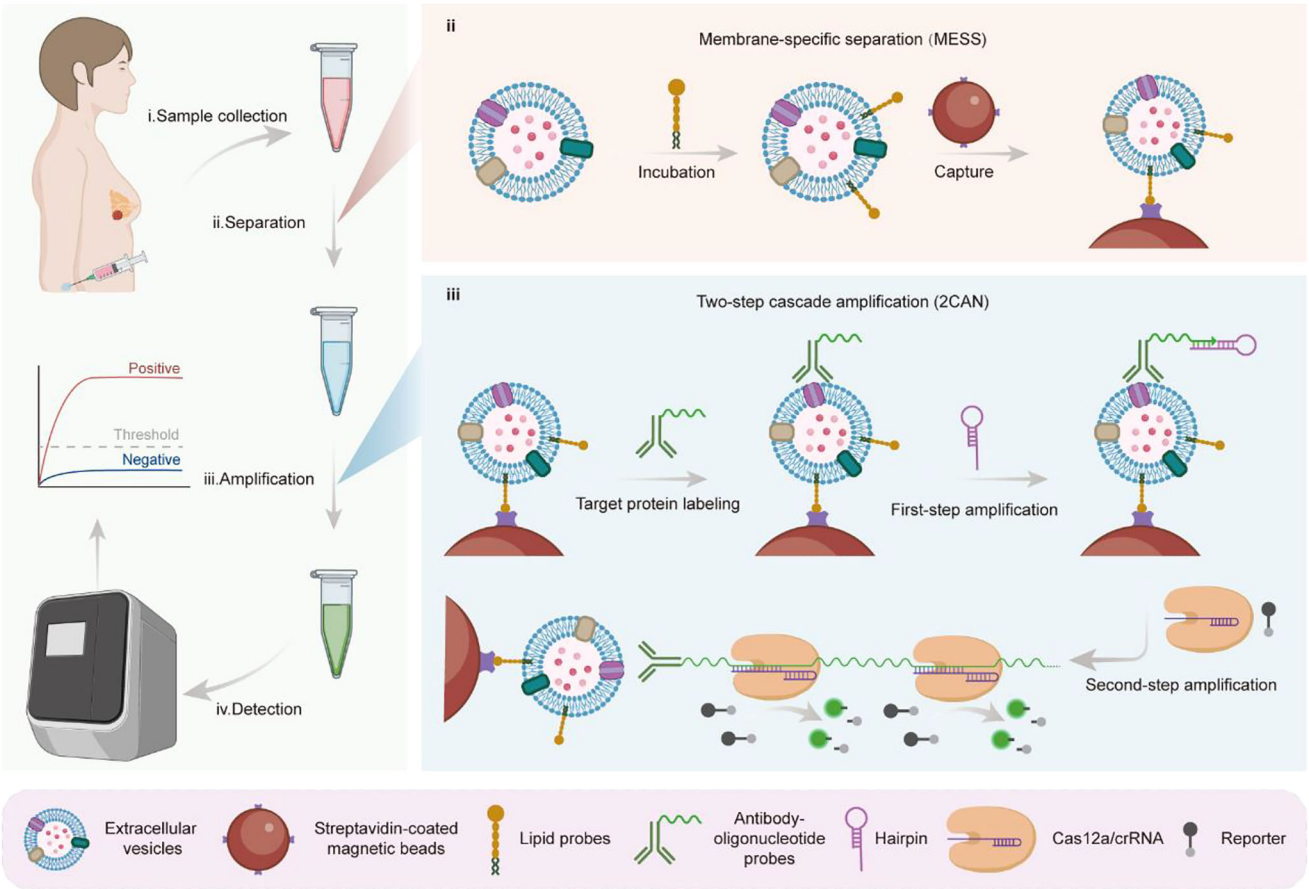

FIGURE 1 Illustration of the MESS2CAN protocol for EV protein analysis and breast cancer detection. Plasma samples are collected from a human subject (i) and then incubated with lipid probes and streptavidin-coated magnetic beads (SA-MBs) for EV separation (ii). Antibody-oligonucleotide probes are used to label the target proteins with oligonucleotides. The oligonucleotides are first amplified through a primer exchange reaction (PER), and further enhanced by a Cas12a system in this two-step cascade amplification (iii). Finally, the EV proteins are quantified by detecting the fluorescence intensity of the reaction solutions with a fluorescence detector (iv).

as important biomarkers for early cancer diagnosis (Pan et al., 2022; Qian et al., 2022; Xu et al., 2018), where the type and expression levels of EV proteins can indicate the cancer classification and progression status (van Niel et al., 2018). However, the small clinical sample volumes, confounded with interference by non-EV components and the normally low expression levels of target proteins pose great challenges for specific EV isolation and protein analysis (Yu et al., 2022), both of which are necessary for an accurate clinical diagnosis.

Among existing EV isolation methods, ultracentrifugation is considered the gold standard, yet it is time-consuming, laborious and requires large initial sample volumes (Witwer et al., 2013). Other approaches, such as filtration, polymer-based precipitation and immunoaffinity capture, commonly suffer from low EV yields and/or poor EV purity and integrity (Merchant et al., 2017). Due to these reasons, they are not practical for clinical applications when only trace amounts of biological samples are available. Similarly, conventional methods of EV protein analysis, such as the western blot and enzyme-linked immunosorbent assay (ELISA) (Shao et al., 2018), have poor sensitivity and require pre-isolation of EVs, limiting their applications in clinical diagnosis. Biosensors have been developed for sensitive detection of EV proteins based on various platforms, such as fluorescence (Mori et al., 2019), surface plasmon resonance (SPR) (Im et al., 2014), electrochemistry (Wang et al., 2017) and colourimetric (Li et al., 2022) methods. However, the sensitivity of most existing biosensors relies on sophisticated instruments and cumbersome signal amplification strategies (Liang et al., 2017). To date, methods of efficient EV isolation and sensitive protein detection are still highly desirable for facile and rapid diagnosis based on EV proteins in clinical samples.

Herein, we have developed a membrane-specific separation and two-step cascade amplification (MESS2CAN) strategy for EV protein detection (Figure 1). We first achieved the membrane-specific separation (MESS) using lipid probes (LPs) and streptavidin-coated magnetic beads (SA-MBs), which allowed indiscriminate capture of EVs onto the surface of SA-MBs, facilitating the direct downstream analysis of EV proteins. We then labelled the captured EVs with oligonucleotides using antibody-oligonucleotide probes. This enables protein detection via nucleic acid sequence detection. For nucleic acid sequence detection, we cascaded two nucleic acid amplification strategies, primer exchange reactions (PER) (Kishi et al., 2018, 2019) and

CRISPR/Cas12a system (Chen et al., 2018; Ke et al., 2022; Swarts & Jinek, 2019) to amplify the oligonucleotides, and detected the target species via a fluorescence detector. We achieved target protein detection with a limit-of-detection of 10 EVs per microliter using MESS2CAN. Moreover, we used MESS2CAN to analyse the expression of HER2, EGFR and EpCAM proteins on EVs from four different breast cancer cell lines, where it exhibited superior performance in detecting lowly-expressed EV surface proteins. We further applied MESS2CAN for protein analysis of EVs sampled from clinical human samples (30 HER2-positive breast cancer (HER2+ BC), 30 triple-negative breast cancer (TNBC) and 30 healthy donors (HD)), where it achieved highly precise and efficient differentiation between these three cohorts.

2 | RESULTS

2.1 | Overview of EV protein analysis for early breast cancer detection via MESS2CAN

Figure 1 is a schematic illustration of EV protein analysis protocol for early breast cancer detection using MESS2CAN. The entire protocol is comprised of four steps: (i) sample collection; (ii) separation; (iii) amplification; (iv) detection. Blood plasma samples collected from human subjects are used for EV separation and protein analysis by MESS2CAN. Using MESS, lipid probes are first incubated with the samples in order to insert their hydrophobic tails into the membranes of EVs. SA-MBs are then added to interact with the biotin heads of lipid probes and capture EVs onto the surface of SA-MBs. Next, antibody-oligonucleotide probes are used to recognise the target proteins and to label them with oligonucleotides. This oligonucleotide sequence is custom-designed with two domains, including a ten-T spacer and a random ten-base sequence which serves as the primer of PER. In the presence of matching hairpins and enzymes, the primer can be extended through PER to form a long single-stranded chain with hundreds of repeating units (first-step amplification). The long single-stranded chain is the target sequence of the Cas12a system. The Cas12a system contains three elements: the Cas12a protein, CRISPR RNA (crRNA) sequences and reporters. The crRNA is comprised of two segments. One segment can specifically bind to the Cas12a protein and the other segment is complementary to the target DNA. The reporter is a 10–12 nt single-stranded DNA (ssDNA) sequence with a quencher at one end and a fluorophore at the other end. It is designed to indicate the amplification results. Under the guidance of the crRNA, the Cas12a protein can specifically recognise the target DNA sequence. After combining with the target sequence, the Cas12a protein is activated to nonspecifically cleave the surrounding ssDNA reporters. This releases fluorophore from the quencher molecule and activates the fluorescence (second-step amplification). Target EV proteins can be quantified by detecting the fluorescence intensity of the reaction solution using a fluorescence detector.

2.2 | Characterisation of the performance of MESS and comparison with standard EV isolation methods (e.g., ultracentrifugation and antibody-based magnetic separation)

EVs from MDA-MB-231 cells were first isolated by ultracentrifugation and used as standard control. Transmission electron microscopy (TEM) showed that the EVs were cup-shaped (Figure 2a). NTA analysis showed that the isolated EVs ranged in size from 30 to 200 nm (Figure 2b) and the corresponding concentration was 1.5×10^{10} particles per μL. Western blot was used to verify the protein expression by EVs and the parental cells, including tetraspanins (CD9, CD81, CD63), TSG101 and calnexin (Figure 2c). Calnexin only existed in parental cell lysate while TSG101, CD63, CD9 and CD81 proteins were expressed in both cell lysate and the EVs, which is consistent with results reported in the literature (Chen et al., 2021; Kumar et al., 2022; Piao et al., 2018).

We then characterised and optimised the MESS process using the obtained EVs. We developed LPs which are long chains linked by PEG2K with biotin heads and hydrophobic tails (DSPE), to capture EVs with SA-MBs (Figure 2d). To verify the capture process of MESS, we labelled EVs and SA-MBs with DiI and fluorescein isothiocyanate (FITC), respectively, and observed them under a confocal laser scanning microscope (CLSM). Free DiI-labelled EVs and bare FITC-labelled SA-MBs were imaged as bright orange dots and green fluorescent spheres, respectively (Figure S1). To demonstrate that the orange fluorescent dots are actual EVs rather than DiI aggregates, we mixed DiI-labelled EVs and EV-free samples with 100 nm green fluorescent polystyrene beads and observed them under CLSM (Figure S2). The orange fluorescent dots appeared only in the EVs group, which were similar in size to green fluorescent beads, while the group of EV-free samples showed no orange fluorescent signal. We then captured the DiI-labelled EVs with FITC-labelled SA-MBs through MESS, and used DiI-labelled EV-free samples as control (Figure 2e). The orange dots (white arrow) overlapping with green spheres were EVs, indicating that EVs were captured onto the surface of SA-MBs through MESS. In addition, the images of scanning electron microscopy (SEM) also verified the successful capture of intact EVs by SA-MBs (Figure S3).

Next, we optimised the LP concentration to achieve the optimum EV recovery rate. We incubated approximately 10^9 DiO-labelled EVs with different concentrations of LPs (0.001, 0.01, 0.1,1,10 μM) and then added a constant number of SA-MBs to pull down the EVs that reacted with LPs. We monitored the fluorescent intensity of EVs captured by SA-MBs at different LP

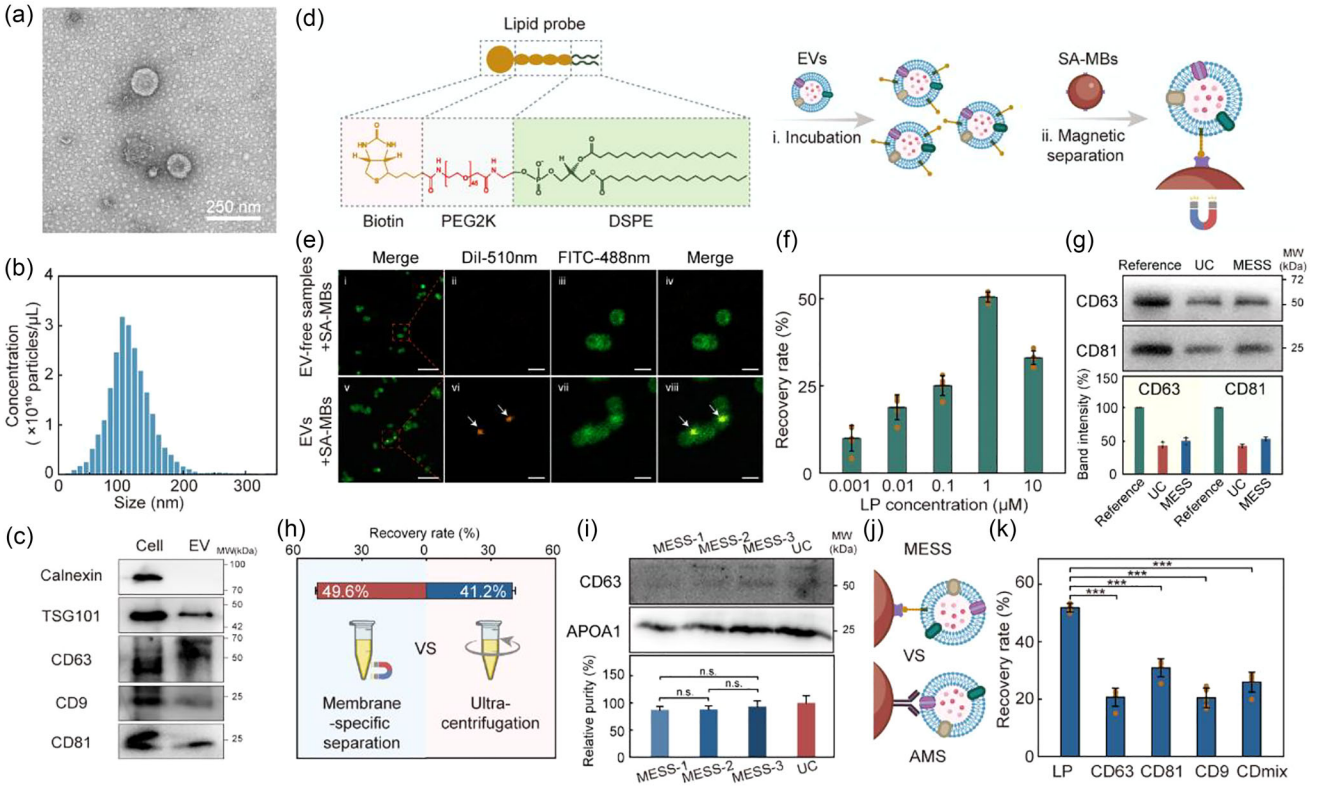

FIGURE 2 Characterization of the performance of the membrane-specific separation (MESS) and comparison with standard EV isolation methods (e.g., ultracentrifugation and antibody-based magnetic separation). (a) TEM image of EVs derived from the MDA-MB-231 cell line by ultracentrifugation. Scale bar: 250 nm. (b) Size distribution and concentration of EVs, as characterised by NTA analysis. (c) The expression of calnexin, TSG101, CD63, CD9 and CD81 in MDA-MB-231 cell lysate and cell-derived EVs by western blot analysis. Equal amounts (15 μg) of total proteins from cells and EVs are loaded into each lane. (d) Illustration of EV capture by MESS. Lipid probes (LPs) are long chains linked by PEG2K, with biotin at one end and DSPE at the other end. LPs are first inserted into the EV membrane and then they are pulled down by SA-MBs, along with the attached EVs, via magnetic separation. e, Confocal fluorescent images of SA-MBs incubated with DiI-labelled EV-free samples (i–iv) and DiI-labelled EVs (v–viii), respectively. The white arrows in (v) and (viii) represent EVs captured by SA-MBs. Scale bars: (i, v) 5 μm, (ii–iv, vi–viii) 1 μm. (f) The EV recovery rate using MESS at different LP concentrations. (g) Western blot analysis of the expression of CD63 and CD81 in EV samples prepared by MESS and ultracentrifugation (UC). Equal volumes (10 μL) of each group were loaded to into the gel. (h) Comparison of the EV recovery rates between MESS and ultracentrifugation (UC). (i) Western blot analysis of CD63 and APOA1 in EV samples isolated from model plasma samples by MESS and UC. MESS-1, MESS-2 and MESS-3 are the groups corresponding to the original amounts of LPs, 5-fold spiked and 25-fold spiked, respectively. Equal volumes (10 μL) of each group were loaded to each lane. (j) Schematic illustration comparing MESS and the antibody-based magnetic separation method (AMS). (k) EV recovery rate of MESS and the AMS method (CD63, anti-CD63-based MS; CD81, anti-CD81-based MS; CD9, anti-CD9-based MS; CDmix, anti-CD63/anti-CD9/anti-CD81-based MS). In all charts, n.s., $p > 0.05$; *$p < 0.05$; **$p < 0.01$; ***$p < 0.001$.

concentrations using a plate reader (Figure S4) and calculated the corresponding EV recovery rates (Figure 2f). With the increase in LP concentration, the EV recovery rate increased gradually to a maximum of 1 μM, followed by a decrease with a further rise in LP concentration. This decrease after 1 μM is likely due to the competition of excess free LP with LP-labelled EVs for binding to SA-MBs. The optimal LP concentration was set at 1 μM with a corresponding EV recovery rate of 49.6%.

In order to compare the performance of MESS and ultracentrifugation (UC) in EV isolation, we used western blots to determine the expression of EV-specific proteins (CD63 and CD81) and assessed their recovery rate. EVs (~6×10^{10}) particles) pre-isolated from MDA-MB-231 cells were divided equally into triplicates, one of which was directly lysed and used as a reference group. The other two were doped into equal amounts of 10% EV-depleted FBS/PBS (v/v) solution as model samples and recovered by MESS and UC, respectively. Equal volume analysis and band intensity ratio were used to assess the recovery rate (Figure 2g and Figure S5). With CD63 and CD81 as target bands, the EV recovery rates of MESS were 50.0 ± 4.8% and 52.9 ± 2.8%, respectively, while the EV recovery rates of UC were 43.0 ± 4.7% and 42.5 ± 2.4%, respectively. The separation efficiency for target proteins were statistically consistent with the EV recovery rate (49.6 ± 1.4%) of DiI-labelled EVs determined by fluorescence, indicating that it is feasible to quantify EV separation efficiency by DiI dyes. To facilitate the comparison of capture efficiency of different methods, we set the capture efficiency of MESS as 49.6% and the corresponding capture efficiency of UC was 41.2% (Figure 2h).

To further assess the performance of MESS in practical applications, we compared the relative recovery rate and purity of EVs isolated by MESS and UC from model plasma samples. Model plasma samples were prepared by spiking (~8×10^{10} particles) pre-isolated EVs into EV-depleted plasma and divided into four replicates, each of which was recovered though MESS

TABLE 1 Comparison of MESS with other EV isolation methods.

Methods	Processing time	EV recovery rate	Data source
Ultracentrifugation	6 h	41.2%	This work
Antibody-based magnetic separation	2 h (37°C) or 14 h (4°C)	29.2%	This work
Polymer-based precipitation	12 h	41%	Reference (Chen et al., 2021)
Size-exclusion chromatography	4.5 h	40%	Reference (Chen et al., 2021)
MESS	1 h	49.6%	This work

or UC. Considering the interference of lipoproteins in plasma, we added two additional groups with increased amounts of LP to investigate the effect of the amounts of LP on the EV recovery rate or purity. MESS-1, MESS-2 and MESS-3 are the groups corresponding to the original amounts of LP, 5-fold spiked and 25-fold spiked, respectively. According to the MISEV 2018 guidelines and reported paper (Chen et al., 2021), we performed western blots to determine the presence of CD63 and Apolipoprotein A1 (APOA1), and used equal-sample-volume analysis to assess the EV recovery rate and purity of each group. CD63, a characteristic protein of EVs, was used to characterise the EV recovery rate of each method by calculating the band intensity of CD63 in each sample (Figure S6). APOA1, a major lipoprotein contaminant in plasma, was selected to assess the purity of each method by calculating the band intensity ratio of CD63 to APOA1 in each sample (Figures 2i and S6). We set both the recovery rate and purity of the UC group as 100%, and calculated the relative recovery rate (50.30% of MESS-1, 65.76% of MESS-2, 77.72% of MESS-3) and relative purity (86.90 % of MESS-1, 87.87% of MESS-2, 93.12% of MESS-3) of other groups. The results showed that the lipoproteins in plasma interfered with the binding of LP to EVs, leading to a decrease in EV recovery. However, this decline could be improved by increasing the amount of LP. In addition, there was no statistical difference ($p > 0.05$) in purity between the three MESS groups, suggesting that the purity of MESS was not affected by the amount of LP. The purity of all three MESS groups was <15% lower than that of UC, indicating that MESS was suitable for subsequent protein analysis. Notably, although higher EV recovery rate of MESS can be achieved by increasing the amount of LP and corresponding SA-MBs, the fluorescence quenching effects of magnetic beads will also be enhanced (Qingqing et al., 2016; Zhang et al., 2017), which will affect the subsequent fluorescence detection of EV proteins. Therefore, the amount of LP and SA-MBs used in MESS-1 group was selected for further EV protein detection applications.

Furthermore, we compared the EV recovery rate for MESS against antibody-based magnetic separation (AMS) (Figure 2j). MESS showed the highest EV recovery rate (49.6%), while EV recovery by AMS varied depending on the quantity of different antigens on the EVs, corresponding to 29.2% for anti-CD81-based MS, 19.3% for anti-CD9-based MS, 19.5% for anti-CD63-based MS and 24.5% for anti-CD81/anti-CD9/anti-CD63-based MS (Figure 2k). Using our data and other data from recent literature, we provided a comparison of MESS with current mainstream EV isolation approaches, by sample processing time and recovery rate (Table 1). MESS presents unique advantages for rapid and efficient EV isolation and an ideal choice for downstream EV analysis.

2.3 | MESS2CAN detects EV surface protein corresponding to 10 EV per microliter sensitivity

After EV isolation using MESS, we adopted three steps to achieve EV protein detection (Figure 3a). First, we labelled the target protein on the EVs with antibody-oligonucleotide probes. We chose CD81 as the target protein and then synthesised the anti-CD81 antibody-oligonucleotide probes (Yan et al., 2021). The probes were verified through SDS-PAGE (Figure S7). Second, we used oligonucleotides as ssDNA primers and amplified the oligonucleotides though PER (Figure 3b). The ssDNA primer with a sequence domain α binds to its complement α^* (step 1) and begins extension with the aid of strand-displacing polymerase (step 2). After extending another α domain, the polymerase halted at the GC pairs due to the absence of dGTP in the reaction. Then, the α domain on the hairpin competes with the copied α domain through branch migration to revert to the original hairpin structure (step 3). Once the replicated domain α is replaced, the extended primer can spontaneously dissociate from the hairpin (step 4) and initiate the next cycle. After repeated cycles, the primers are extended into long single-stranded nucleic acids with repeated α domains with the aid of catalytic hairpins and strand-displacing polymerases. We validated the PER products by agarose gel electrophoresis (Figure 3c). We also modulated the lengths of the PER products by changing the polymerase concentration, hairpin concentration, primer concentration and incubation time (Figures S8 and 3c). Under optimised reaction conditions (1 μM hairpin, 0.8U μL^{-1} polymerase and 2 h incubation time), the lengths of PER products increased with reduction in primer concentration (Figure 3c). At a primer concentration of 0.125 μM, the product length increased to ~1500 base pairs, which is approximately 150 times the primer length. These results indicated that PER could provide at least 150-fold signal amplification.

In the third and final part of the detection process, after the extension of the oligonucleotides by PER, we conducted a second-step amplification using the CRISPR-Cas12a system. The crRNA is exactly complementary to the two domain α regions and able to guide the Cas12a protein to recognise the amplified sequences. Upon binding to the PER products, the Cas12a polymerase

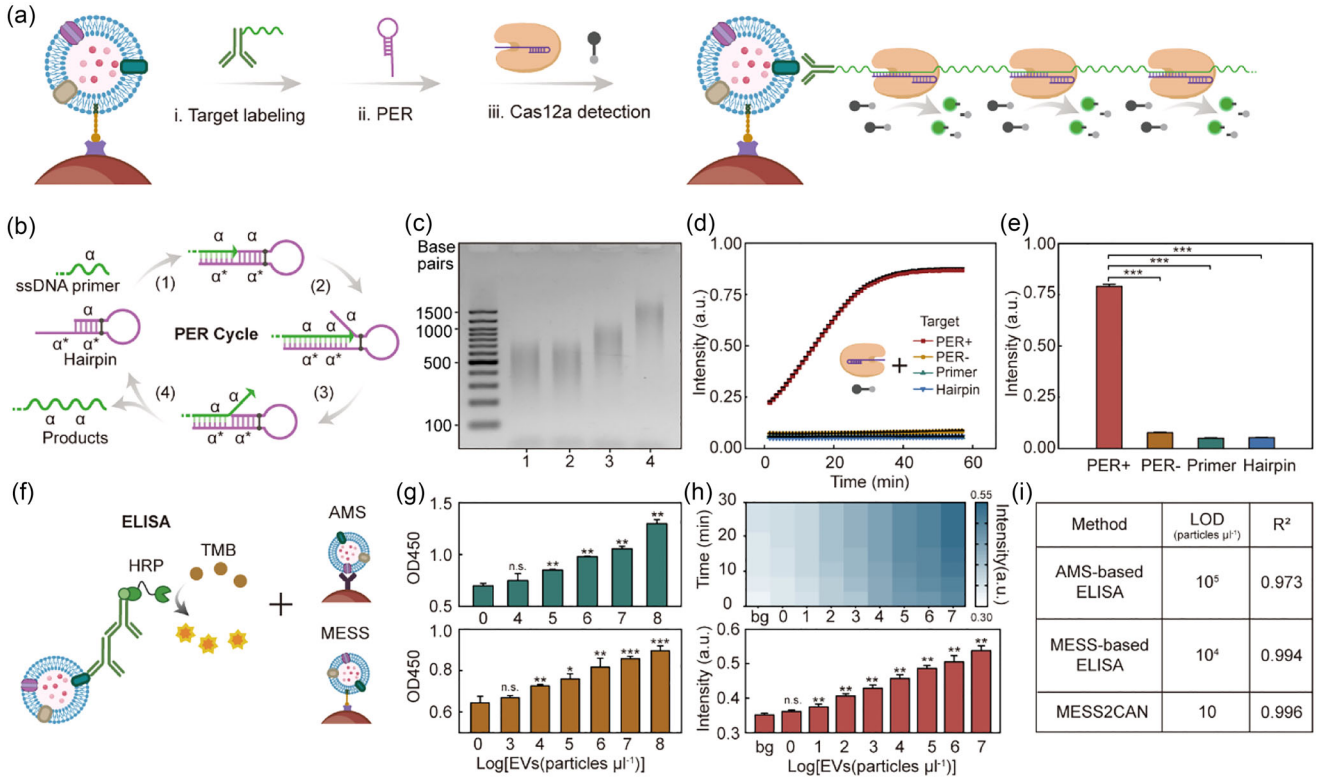

FIGURE 3 MESS2CAN detects EV surface protein corresponding to 10 EV per microliter sensitivity. (a) Schematic of target labelling and the two-step cascade amplification. After MESS, the captured EVs are labelled with an oligonucleotide through antigen-antibody reaction. Following PER (first-step) and Cas12a cascade (second-step) amplification, the fluorescent signal corresponding to labelled EV proteins is detected using a fluorescence detector. (b) Schematic of the PER cycle. (1) primer binding, (2) strand displacing elongation, (3) branch migration, and (4) dissociation. (c) 1% agarose gel electrophoresis of PER products with different primer concentrations. Lanes 1–4 are PER products with primer concentration of 1 μM, 0.5 μM, 0.25 μM, and 0.125 μM, respectively. Other conditions: 1 μM hairpin, 0.8 U μL^{-1} polymerase, and 2 h incubation time. (d and e) Real-time fluorescence kinetic measurements (d) and end-point fluorescence intensity (e) of CRISPR-Cas12a with different targets: primer, hairpin, PER- (PER products without primers), PER+ (PER products), respectively. (f) Illustration of the ELISA assay with antibody-based separation (AMS) and MESS for EV detection. (g) Histograms of the absorbance at 450 nm for serial EV concentrations detected by AMS-based ELISA (top) and MESS-based ELISA (bottom). (h) Heatmap of the time-dependent fluorescence intensity (top) and histogram of the end-point fluorescence intensity (bottom) for serial EV concentrations, as detected by MESS2CAN. In the charts, bg represents background. (i) Limits of detection (LOD) for the three listed methods. In all charts, n.s., $p > 0.05$; *$p < 0.05$; **$p < 0.01$; ***$p < 0.001$.

was activated to cleave the ssDNA reporters and release the fluorophores. We verified the target specificity of the Cas12a system, whereby fluorescence intensity increased rapidly only in the PER+ group with longer reaction time, and negative control groups including primer, hairpin, and PER- all showed background fluorescence intensity (Figure 3d,e).

Next, we applied the MESS2CAN to EV protein detection and compared its detection limit with ELISA. Cell-derived EVs (10^8 particles μL^{-1}) with different serial dilutions were used as simulated samples and CD81 was selected as the target protein. The performances of AMS-based ELISA (top) and MESS-based ELISA (bottom) were compared by measuring the absorbance at 450 nm for EV samples with different concentrations (Figure 3f-g). We also measured fluorescence intensity for serial EV concentrations by MESS2CAN (Figure 3h). The detection limit of each method was calculated (Figure S9), showing that MESS2CAN was able to detect 10 EV particles per microliter (Figure 3h), three orders of magnitude lower than MESS-based ELISA and four orders of magnitude lower than AMS-based ELISA. Using this data and other recent evidence, we compared the detection process for MESS2CAN with other prevalent methods for EV detection (Table 2). MESS2CAN exhibits excellent performance in EV protein detection, providing increased sensitivity coupled with convenience of operation, and without requirement for additional sophisticated equipment. These characteristics make it particularly suitable for EV protein detection in applications of in vitro diagnostics using small amounts of biological samples and/or samples with low EV content.

2.4 | Protein analysis of EVs from four breast cancer cell lines by MESS2CAN

To test MESS2CAN in an example application, we applied the MESS2CAN for protein analysis of EVs derived from four breast cancer cell lines (SK-BR-3, MCF-7, MDA-MB-231, MCF-10A) and compared its performance with fluorescence imaging

TABLE 2 Comparison of different methods for EV detection.

Detection method and Reference	Capture method	Amplification strategy	Required equipment	Limit of detection (particles μL^{-1})
Colorimetric (He et al., 2017)	Anti-CD9 antibody-based capture	HCR+HRP	UV-vis spectrometry	2.2×10^3
Electrochemistry (Guo et al., 2020)	EpCAM aptamer-based capture	HRP	CHI 660D electrochemical workstation	1.3×10^3
Electrochemistry (Park et al., 2021)	Anti-CD63, anti-CD9 and anti-CD81 antibodies- based capture	HRP	Automated HiMEX reader	10
Surface plasmon resonance (Yildizhan et al., 2021)	Anti-CD63 and anti-CD9 antibodies- based capture	Gold nanoparticle-assisted signal amplification	FOx Biosystems	3.125×10^4
Surface-enhanced Raman spectroscopy (Wang et al., 2020)	Anti-CD63 antibody-based capture	Gold nanoparticle-based nanotag	WITec Alpha300 R microspectrometer	100
Fluorescence (He et al., 2022)	Aptamer-based capture	RCA	Hitachi F-4500 spectrofluorometer	42.22
This work	Membrane-specific separation	PER+CRISPR	Roche Light Cycler 96	10

Abbreviations: HCR, hybridization chain reaction; HRP, horseradish peroxidase; RCA, rolling circle amplification.

(Figure 4a). For fluorescence imaging, we first labelled three target proteins (HER2, EpCAM, EGFR) on both cells and cell-derived EVs with the corresponding primary and fluorescent secondary antibodies, and then observed them under CLSM. The expression level of each protein was assessed by its respective fluorescence intensity (Figure 4b) and was verified by western blot (Figure 4c). The expression levels of all three labelled proteins were shown to be consistent between each cell line and its corresponding EVs. Specifically, cell lines with higher expression of a particular target protein (HER2 for SK-BR-3; EpCAM for MCF-7; EGFR for MDA-MB-231) also showed higher fluorescence intensity for that protein on their corresponding EVs. Conversely, cell lines with low or no expression of a target protein showed low or background fluorescence intensity for that protein on their corresponding EVs. We then analysed the fluorescence intensity of each target protein on EVs derived from each of the four cell lines (Figure 4d) and calculated the relative protein expression levels compared to control, target protein-negative EVs (HER2-negative, MDA-MB-231 derived EVs; EpCAM-negative, MCF-10A derived EVs; EGFR-negative, MCF-7 derived EVs). Statistical results (Table S1) demonstrated that EVs with high target protein expression had over 3-fold higher expression levels than the controls, while EVs with low target protein expression had less than 2-fold higher expression levels than the controls.

We then used MESS2CAN to analyze the expression levels of the same target proteins HER2, EpCAM and EGFR on EVs derived from the four cell lines (Figure 4e,f), where expression level was correlated with fluorescence intensity. MESS2CAN was able to distinguish EVs with high, low, or no expression of target proteins with significant sensitivity ($p < 0.001$) (Figure 4f). In order to compare the performance of MESS2CAN against fluorescence imaging, we normalised the expression levels of HER2, EpCAM and EGFR measured by both methods and investigated the correlation of the measurements (Figure 4g). The correlation coefficients (0.950 for HER2, 0.987 for EpCAM and 0.991 for EGFR) suggested that MESS2CAN was as effective as fluorescence imaging in measuring EV protein expression levels. Moreover, MESS2CAN showed an increase of target protein expression levels by more than 10% over fluorescence imaging for EVs with low target protein expression, suggesting that MESS2CAN is particularly advantageous for detecting lowly-expressed proteins.

2.5 | EV protein analysis using MESS2CAN for differentiation between clinical samples from HER2+ BC, TNBC and HD

We demonstrated a practical application of MESS2CAN for EV protein analysis in breast cancer diagnosis (Figure 5a). We first validated the sensitivity of MESS2CAN for tumour marker-positive (HER2-, EGFR- and EpCAM-positive) EVs in spiked plasma samples (Figure S10). Spiked plasma samples were prepared by adding HER2-, EGFR- and EpCAM-positive EVs to the plasma from healthy donors at different dilutions. The limits of detection of MESS2CAN for HER2-, EGFR- and EpCAM-positive EVs were calculated to be 363, 417 and 182 particles μL^{-1}, respectively, which was sufficient for EV protein analysis in plasma. Then we collected 90 clinical test samples from human subjects, with 30 from HER2-positive breast cancer patients (HER2+ BC), 30 from triple-negative breast cancer patients (TNBC), and 30 from healthy donors (HD). There was no significant difference in gender or age between the three groups. 10 μL plasma from each test sample was analyzed by MESS2CAN to quantify the expression

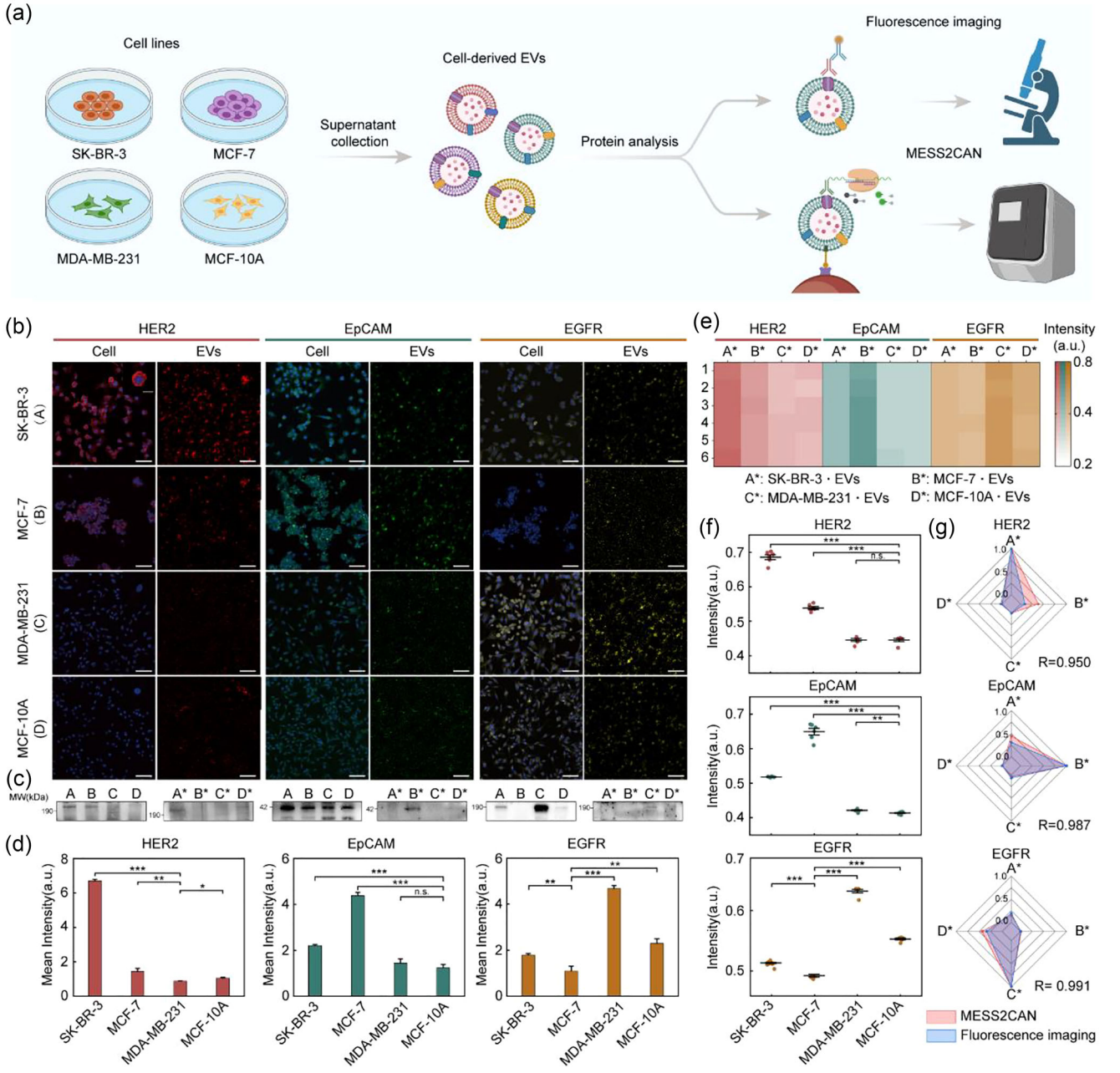

FIGURE 4 Protein analysis of EVs from four breast cancer cell lines by MESS2CAN. (a) Schematic of protein analysis of cell-derived EVs by MESS2CAN and fluorescence imaging. (b) Fluorescence images of antibody-labelled cells and EVs. Proteins HER2, EpCAM and EGFR are shown in red, green and yellow, respectively. Cell nuclei were stained with DAPI and are shown in blue. Scale bar, 20 μm for cell and 2.5 μm for EVs. (c) Validation of the expression of three antigens (HER2, EpCAM, EGFR) on the cells and on cell-derived EVs by western blot. Cell lines SK-BR-3, MCF-7, MDA-MB-231 and MCF-10A are denoted by A, B, C and D, respectively; corresponding EVs are denoted by A*, B*, C* and D*. (d) Statistical histograms of the mean fluorescence intensity of HER2, EpCAM and EGFR on EVs derived from each of the four cell lines. The mean intensity ($n = 5$) was calculated according to the fluorescence images in (b). (e and f) Heatmap (e) and scatter plots (f) of the fluorescence intensity of HER2, EpCAM and EGFR on EVs derived from each of the four cell lines, as measured using MESS2CAN. (g) Radar plot showing the expression levels of HER2, EpCAM and EGFR measured by MESS2CAN (red) and CLSM (blue), where EVs from SK-BR-3, MCF-7, MDA-MB-231 and MCF-10A cell lines are denoted by A*, B*, C* and D*, respectively. The consistency of the results measured using MESS2CAN and CLSM was evaluated by a Pearson Correlation analysis. R-value is indicated in the chart. In all charts, n.s., $p > 0.05$; *$p < 0.05$; **$p < 0.01$; ***$p < 0.001$.

levels of HER2, EGFR and EpCAM (Figure 5b). The expression of HER2 in the HER2+ BC group was significantly higher than that in the TNBC and HD groups, while the TNBC group showed the highest expression of EGFR (Figure 5c). Moreover, both breast cancer (BC) groups (HER2+ BC and TNBC) showed higher expression of EpCAM than the HD group. We then evaluated the diagnostic performance of the three protein markers via an analysis of their receiver operating characteristic (ROC) curve (Figure 5d) and presented their area under the curve (AUC) values (Figure 5e). EpCAM on the EVs showed superior diagnostic

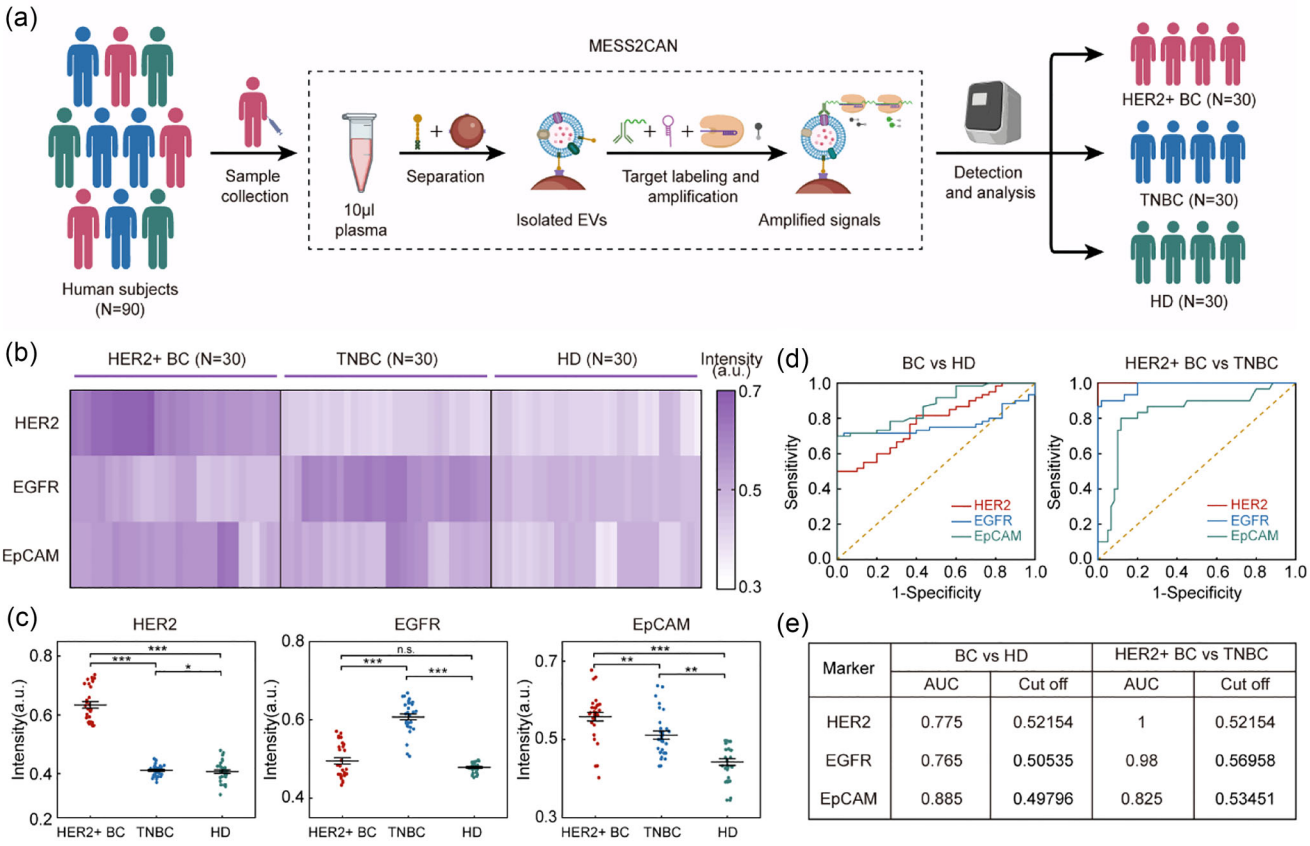

Marker	BC vs HD		HER2+ BC vs TNBC	
	AUC	Cut off	AUC	Cut off
HER2	0.775	0.52154	1	0.52154
EGFR	0.765	0.50535	0.98	0.56958
EpCAM	0.885	0.49796	0.825	0.53451

FIGURE 5 EV protein analysis by MESS2CAN for differentiation between clinical samples from HER2+ BC, TNBC, and HD. (a) Schematic of the EV protein analysis by MESS2CAN for differentiation between clinical samples from HER2+ BC, TNBC and HD. HER2+ BC, HER2-positive breast cancer. TNBC, triple negative breast cancer. HD, healthy donors. EVs in 10 μL plasma were first isolated by MESS and then labelled with antibody-oligonucleotide probes. After two-step amplification, the resulting signal was detected using a fluorescence detector. (b) Heatmap showing the expression levels of HER2, EGFR and EpCAM on EVs from all human subjects. (c) Statistical differences in HER2, EGFR and EpCAM expression on EVs from HER2+ BC, TNBC and HD. (d) ROC curve evaluating the diagnostic ability to differentiate between HER2+ BC, TNBC and HD using three protein markers. (e) AUC value of the ROC curves showing the accuracy of the three markers in differentiating BC from HD, as well as HER2+ BC from TNBC. The corresponding cut off values are shown in the table. In all charts, n.s., $p > 0.05$; $^{*}p < 0.05$; $^{**}p < 0.01$; $^{***}p < 0.001$.

performance in discriminating the two BC groups from the HD group (AUC = 0.885, cut off value = 0.49796). HER2 and EGFR on the EVs showed high sensitivity and specificity in differentiating the HER2+ BC group from the TNBC group (AUC = 1 with cut off value = 0.52154 for HER2; AUC = 0.98 with cut off value = 0.56958 for EGFR). Our findings suggested that HER2, EpCAM and EGFR on EVs could be practical protein biomarkers for breast cancer diagnosis. This also demonstrated the potential of MESS2CAN in providing sensitive and specific analysis of EV proteins for in vitro diagnostics.

3 | DISCUSSION

Tumour-derived proteins on EVs are promising biomarkers for early cancer diagnosis in liquid biopsies. However, current methods are limited in providing rapid, convenient and sensitive detection of EV proteins in trace clinical samples. Herein, we have demonstrated MESS2CAN for direct detection of surface proteins on both cell-derived EVs and plasma EVs. In this method, we first captured EVs with lipid probes and magnetic beads through membrane-specific separation. This enabled non-specific EV capture and achieved a 49.6% EV yield within 1 h from mock cell culture medium (10% EV-depleted FBS in PBS), which was 8.4% higher than ultracentrifugation. For isolation of plasma EVs, the lipoproteins interfered with the bindings of LP to EVs and led to the decrease in EV capture efficiency of MESS. However, this decrease could be improved by increasing the amounts of LP, which was also verified by Wan et al. (2017). In addition, the purity of MESS was only <15% lower than that of ultracentrifugation and not affected by the amounts of LP, indicating that MESS was suitable for protein analysis.

For EV protein detection, we used antibody-oligonucleotide probes to recognise the target EV protein after MESS, which converted protein detection to nucleic acid detection. Although low-cost nucleic acid aptamers have been developed for protein recognition, they still face challenges of few targets and limited affinity (Rothlisberger & Hollenstein, 2018). Therefore, we

used antibodies for antigen recognition in this work. The antibody-conjugated oligonucleotides served as primers for PER and triggered the PER cascaded Cas12a system, leading to the two-step signal amplification.

Using MESS2CAN, we completed the whole process of target EV protein detection within 4 h, and demonstrated a detection limit of 10 EV particles per microliter. Comparing to other methods listed in Table 2, MESS2CAN achieved extremely low EV detection limit without requiring any sophisticated instruments or tedious procedures, having great application prospects in clinical diagnosis. Using MESS2CAN to analyze protein expression of HER2, EpCAM and EGFR on the EVs from four different breast cancer cell lines, we successfully differentiated EVs with high, low and no expression of each target protein. Notably, MESS2CAN showed significant benefit in detecting lowly-expressed proteins since the two-step amplification strategy enabled efficient amplification of weak signals. Finally, we applied MESS2CAN in protein analysis of EVs from 90 clinical test samples and validated the diagnostic performance of using a HER2, EGFR and EpCAM tri-protein panel in differentiating between HER2+ BC, TNBC and HD samples. In this practical application, MESS2CAN achieved EV protein detection from clinical breast cancer samples with high sensitivity, efficiency (less than 4 h operation time), and ease of operation, which is also suitable for the diagnostics of other diseases based on EV protein biomarkers (such as GPC1 (Melo et al., 2015) and EphA2 (Liang et al., 2017) for pancreatic cancer; PSA (Liu et al., 2019) for prostate cancer; CA125 (Liu et al., 2019) for ovarian cancer; LprG for tuberculosis).We believe MESS2CAN holds significant potential to be a routine clinical assay for early disease screening.

4 | MATERIALS AND METHODS

4.1 | Cell culture and isolation of cell-derived EVs by ultracentrifugation

Human breast cancer cell lines (SK-BR-3, MCF-7, MDA-MB-231) were purchased from the Cell Bank of the Chinese Academy of Sciences, Shanghai, and the human mammary epithelial cell line (MCF-10A) was purchased from Shenzhen Hitouch Technology Co.,Ltd. SK-BR-3, MCF-7 and MDA-MB-231 cells were cultured in DMEM medium (Hyclone) with 10% (v/v) EV-depleted fetal bovine serum (FBS; SeraPro) and 1% (v/v) penicillin/streptomycin. The MCF-10A cells were cultured in RPMI-1640 medium (Hyclone) with 10% (v/v) EV-depleted FBS and 1% (v/v) penicillin/streptomycin. All cells were cultured at 37°C with 5% CO_2. Cell culture supernatants were harvested when cells reached a confluency of 70%–80%.

The collected supernatant medium (400 mL) was centrifuged at 300 and 2000 × *g* for 10 min each to remove dead cells and cell debris. The supernatant was then centrifuged at 10,000 × *g* for 60 min and filtered through a 0.22 μm membrane (Millipore). After filtration, the processed supernatant was ultracentrifuged at 100,000 × *g* for 2 h. The resulting precipitates were resuspended in phosphate-buffered saline (PBS) and ultracentrifuged again at 100,000 × *g* for 2 h. Finally, EVs were obtained by suspending the precipitates in 200 μL PBS, and stored at −80°C until further use.

4.2 | TEM and SEM

A 10-μL drop of freshly isolated EVs (~ 10^9 particles μL^{-1}) was added to a copper grid and incubated for 1 min, after which the droplet was blotted dry with filter paper. The adsorbed EVs were stained with phosphotungstic acid (3%) for 50 s and then blotted dry with filter paper. The morphologies of the EVs were observed using TEM (Tecnai G2, Thermofisher). One microlitre bare SA-MBs and SA-MBs with captured EVs were diluted 100-fold and added to the silicon wafer, respectively. After natural drying, samples on the silicon wafers were imaged using SEM (JSM-7800F, JEOL).

4.3 | NTA

The size distribution and concentration of EVs were measured by Nanoparticle Tracking Analysis (NTA) (Zetaview, Particle Metrix). All EV samples were diluted in PBS to ~10^7 particles mL^{-1} and measured at room temperature according to the manufacturer's instructions.

4.4 | Protein extraction and quantification of cells and EVs

Proteins of cells and EVs were extracted through the following steps. First, the sample of cells or EVs was incubated with 100 μL lysis buffer (1×RIPA buffer with 1 mM phenylmethanesulfonyl fluoride and 1× Protease inhibitor cocktail, Beyotime) on ice

for 30 min. Then the mixture was centrifuged at 12,000 × *g* for 10 min. The supernatant was finally retained and the protein concentration was quantified through BCA assay (Pierce™BCA Protein Assay, ThermoFisher).

4.5 | Western blot

For western blot analysis, each sample containing 15 μg proteins and 1× protein loading buffer (Tanon) was fisrt heated at 95°C for 10 min. Then all samples were loaded separately into different lanes of a 10% PAGE gel which was pre-prepared using the PAGE Gel Quick Preparation Kit (10%) (Yeasen). Using 1× SDS-PAGE running buffer (Servicebio), the proteins were concentrated at 80 V for 30 min and then separated at 120 V for 60 min. After separation, the proteins were transferred from the gel onto a polyvinylidene difluoride membrane (Bio-Rad) in the transfer buffer (Servicebio, with 20% v/v methanol) at 100 V for 90 min. For blocking of the membrane, 3%−5% (w/v) skim milk in 1× TBST buffer (Servicebio) was prepared and incubated with the membrane at room temperature for 1 h. Washed three times with 1× TBST buffer for 10 min each, the membrane was then incubated with different primary antibodies at 4°C overnight. After incubation, the membrane was washed again with the same procedure described above. To detect the primary antibodies on the membrane, the Peroxidase-conjugated goat anti-mouse or anti-rabbit secondary antibodies were used to incubate with the membrane at room temperature for 1 h. After washing three times with 1× TBST buffer, antibody-related chemiluminescence signals on the membrane was finally observed under the Tanon system (Tanon-5200s). The primary antibodies were diluted in 1× TBST buffer containing 3% (w/v) BSA at a dilution ratio of 1:1000. All the primary antibodies (Anti-CD63: #353108, Biolegend; anti-CD9: #312112, Biolegend; anti-CD81: #349514, Biolegend; anti-EpCAM: #324202, Biolegend; anti-EGFR: #933902, Biolegend; anti-HER2: #324402, Biolegend; anti-calnexin: #2679T, Cell Signaling Technology; anti-TSG101:72312S, Cell Signaling Technology; anti-APOA1: ab300085, Abcam) and secondary antibodies (Goat anti-mouse antibody: #33201ES60, Yeasen; goat anti-rabbit antibody: #33101ES60, Yeasen) were diluted in 1× TBST buffer containing 3% (w/v) BSA at a dilution ratio of 1:1000.

4.6 | Fluorescent labeling of EVs and calculation of recovery rate

In order to label EVs with 3,3′-dioctadecyloxacarbocyanine perchlorate (DiO), pre-isolated EVs from MDA-MB-231 cells (100 μL, ~ 10^9 particles μL^{-1} in PBS) were first incubated with a DiO working solution (100 μL, 5 μM in PBS) for 30 min and protected from light exposure at room temperature. Next, the mixture was centrifuged 5 times at 6000 × *g*, for 5 min each time, with an ultrafiltration tube (100 kDa MWCO, Millipore) at 4°C. Purified DiO-labelled EVs were quantified by NTA analysis and stored at 4°C in the dark.

In order to calculate the EV recovery rate, 10^9 DiO-labelled EVs were spiked into EV-depleted FBS (10% v/v in PBS) as mock samples. The fluorescence intensity of samples was recorded by a plate reader (BioTek) before and after the capture of EVs through MESS or AMS. The difference in fluorescence intensity before and after EV capture is the fluorescence intensity of EVs captured by each method. The EV recovery rate was calculated through the formula:

$$\text{Recovery rate } (\%) = \frac{(\text{FI}_{\text{bf}} - \text{FI}_{\text{af}}) - \Delta FI_{bg}}{FI_{bf}}$$

FI_{bf} and FI_{af} represent the fluorescence intensity of the EV samples before and after the capture process, respectively. ΔFI_{bg} represent the background fluorescence intensity obtained by non-specific adsorption of EVs by bare magnetic beads.

4.7 | Fluorescent labelling of proteins on cells and EVs

First, 10,000 cells were cultured in 96-well plates for 12 h and then washed two times with PBS. Cells were fixed by incubating with 100 μL of pre-chilled 4% (w/v) paraformaldehyde (Aladdin) for 20 min at room temperature. After washing three times with PBS, cells were further incubated with 0.2% (w/v) Triton X-100 (ThermoFisher) for 15 min, followed by blocking with 3% bovine serum albumin (BSA) for 15 min. The treated cells were then ready for fluorescent labelling.

In order to label the proteins on cells, the aforementioned processed cells were first incubated with 100 μL of primary antibody solutions at 4°C overnight. After washing three times with 0.01% Tween 20 in PBS (PBST), the cells were incubated with Alexa Fluor 594-conjugated secondary antibody solution for 1 h at 37°C in the dark. Primary and secondary antibody solutions were prepared by diluting the primary antibodies (anti-HER2, anti-ECAM and anti-EGFR; Biolegend, clone No's 24D2, 9C4, A19002A, respectively) and fluorescent secondary antibody (Yeasen) with 3% BSA/PBS at a ratio of 1:200, respectively. After incubation,

cells were washed three times with PBST and incubated with DAPI for 20 min. After washing three times with PBST, the cells were stored in the dark until further use.

In order to label the proteins (HER2, EpCAM and EGFR) on EVs, EVs (100 μL, ~ 10^9 particles μl^{-1} in PBS) derived from four different cell clines were first incubated with primary antibodies (5 μL, 1 mg mL^{-1} in 2% BSA/PBS solution) at 4°C overnight. After incubation, EVs were purified by centrifugation at 6000 × *g* for 5 min in ultrafiltration tubes (300 kDa MWCO, Pall) to remove any free primary antibodies. After three times of ultrafiltration, Alexa Fluor-488-labelled secondary antibodies were added and incubated with the EV samples for 2 h at room temperature in the dark. Excess secondary antibodies were removed by ultrafiltration three times using the same procedures as above. The purified EVs were quantified by NTA and stored in the dark prior to fluorescence imaging.

4.8 | Fluorescence imaging of cells and EVs

Cells and EVs were both observed using a Zeiss LSM800 Confocal Microscope. The treated cells in 96-well plates and were imaged with a 10X objective lens. To image the EVs, 10 μL of DiO-labelled EVs were dropped onto a glass slide, covered with a coverslip and then imaged with a 63X oil-immersion lens.

4.9 | Membrane-specific separation of EVs

Lipid probes (DSPE-PEG2K-biotin; Aladdin) were dissolved in absolute ethanol and prepared as 1 mM stock solution. Similar to the PKH26 labeling protocol, Diluent C was used as a solvent for lipid probes to label EVs. Lipid probes were first diluted to a desired concentration by Diluent C and then incubated with 100 μL EV samples (20 μL EV-spiked samples with 80 μL Dliuent C) for 30 min at 4°C. Next, 20 μL of 50 mg mL^{-1} SA-MBs were added and incubated with the mixture for 30 min at room temperature. After incubation, the SA-MBs were washed three times with PBS and resuspended in stock solutions (0.1% BSA in PBS) at 4°C for further protein detection. To optimise the LP concentration, DiO-labelled EVs were used to incubated with LPs (final concentration of 0.001, 0.01, 0.1,1,10 μM). The EV recovery rates at different LP concentrations were calculated according to the previous steps. The LP concentration corresponding to the maximum EV recovery was the optimal concentration for subsequent experiments.

4.10 | Antibody-based magnetic separation (AMS) of EVs

Antibody-coated magnetic beads were prepared by incubating SA-MBs (100 μL, 10 mg mL^{-1}) with 20 μg biotin-labelled antibodies (biotin anti-human CD63, CD9, CD81 antibodies; Biolegend, clone No's H5C6, HI9a, 5A6 respectively) in PBS for 1 h at room temperature. The beads were blocked with 5% BSA/PBS for 2 h before use. To isolate EVs, 20 μL of 10 mg mL^{-1} antibody-coated magnetic beads were incubated with 100 μL of EV samples at 4°C overnight. The mixture was washed three times with PBS and then stored at 4°C.

4.11 | Synthesis and validation of antibody-oligonucleotide probes

Antibody-oligonucleotide probes were generated by conjugating the thiol-modified oligonucleotide to an antibody using sulfosuccinimidyl 4-(N-maleimidomethyl) cyclohexane-1-carboxylate (Sulfo-SMCC; Thermo Fisher Scientific). The antibody (40 μg) was first purified with an ultrafiltration tube (50 kDa MWCO, Millipore) and resuspended in conjugation buffer (sodium phosphate buffer, pH 7.2) at a final concentration of 1 mg mL^{-1}. The antibody was then mixed with 4 μL of freshly prepared Sulfo-SMCC (4.8 mg mL^{-1} in double distilled water) and reacted for 2 h at 4°C. After this reaction, the treated antibody was ultrafiltered three times at 12,000 × *g* to remove any excess Sulfo-SMCC molecules. Meanwhile, the thiol-modified oligonucleotides (100 μM, 10 μL) were reduced by Tris(2-carboxyethyl)phosphine (TCEP·HCl, 10 mM, 10 μL; ThermoFisher) for 1 h at 37°C and purified with an ultrafiltration tube (3 kDa MWCO; Millipore) at 12,000 × *g* and this was repeated three times. Then the purified antibodies and oligonucleotides were mixed at a 1:3 molar ratio and reacted for 14–16 h at 4°C in the dark. The reaction solution was then washed three times by ultrafiltration (12,000 × *g*, 5 min) to obtain the purified probes.

In order to validate the generation of antibody-oligonucleotide probes, 10% SDS-PAGE gel (Yeasen) was prepared according to the manufacturer's instructions. Equal amounts (100 ng) of free antibodies and synthesised probes were loaded onto the gel. The SDS-PAGE gel was stained with Coomassie Brilliant Blue (Beyotime) for 2 h and decolorised with double distilled water for

2 h. Synthesised probes were then stored in stock buffer (0.1% BSA, 0.05% Tween, 0.1 μg μL^{-1} salmon sperm DNA, 100 nM goat IgG, 1 mM D-biotin, and 5 mM ethylene diamine tetraacetic acid in PBS).

4.12 | Primer exchange reaction (PER)

The primer/hairpin/clean.G sequences (listed in Table S1) were designed according to the cited publication (Kishi et al., 2018) and obtained from Sangon Biotech (Shanghai) Co., Ltd. A solution volume of 20 μL (containing final concentration of 0.125–1 μM primer, 0.125–1 μM hairpin, 0.2–0.8 U μL^{-1} Bst Large fragment polymerase, 1 mM dATP/dCTP/dTTP, 100 nM clean.G 10 mM $MgSO_4$; Yeasen) was prepared, and reacted at 37°C for 0.5–2 h. Clean.G was used to eliminate possible dGTP in the dATP/dCTP/dTTP mixture. Specifically, 20 μL PER reactions without primers were first incubated at 37°C for 15 min to remove any interfering dGTP. Primers were then added and the reaction mix was incubated at 37°C for another 0.5–2 h. After incubation, the reaction was halted by heating the mixture at 80°C for 20 min. PER products regulated by the reaction time, the concentrations of primer, hairpin and polymerase were verified through 1% agarose gel electrophoresis.

4.13 | Cas12a detection

CrRNA and ssDNA reporters (listed in Table S1) were designed according to the reference (Ke et al., 2022) and produced by Sangon Biotech (Shanghai) Co., Ltd. The 20 μL reactions of the Cas12a system contained five components: 1 μL LbaCas12a protein (1 μM; New England Biolabs, Inc.), 1 μL crRNA (1 μM), 1 μL ssDNA reporter (2 μM), 2 μL NEBuffer 2.1 (New England Biolabs, Inc.), 2 μL target sequences and 13 μL double distilled water. The reactions were incubated for 0.5–1 h at 37°C and the fluorescence intensity of reactions was monitored every minute with a LightCycler 96 (Roche, Switzerland).

4.14 | ELISA assays based on membrane-specific separation and antibody-based separation

Isolated EVs (captured by membrane-specific separation and antibody-based separation) were first incubated with 100 μL anti-human CD81 antibodies (5 ng μL^{-1} in 3% BSA/PBS) for 12 h at 4°C. After washing three times with PBS, horseradish peroxidase (HRP)-linked secondary antibody (1 ng μL^{-1} in 3% BSA/PBS) was added and incubated with the mixture for another 1 h at 37°C. After washing another three times with PBS, 100 μL freshly prepared TMB substrates (component A: component B = 1:1; Sangon Biotech (Shanghai) Co., Ltd.) were added. The mixture was then transferred to 96-well plates, incubated at 37°C for 5–30 min, and quantified by detecting the absorbance at 450 nm.

4.15 | Clinical samples

Blood plasma samples were collected at Changhai Hospital, Shanghai. The sample collection complied with relevant ethical regulations (Ethics number: CHEC2020-106). All donors signed a written informed consent prior to sample collection and use in research. All patients were diagnosed through tissue biopsy and their clinical characteristics were shown in Table S3. The whole blood samples were collected in anticoagulation tubes and immediately centrifuged at 1550 × *g* for 10 min at 4°C to obtain the cell-free plasma samples. All plasma samples were transported on dry ice, and stored at −80°C before and after transportation until further use. Before isolating EVs through different methods, Plasma samples were first purified at 10,000 × *g* for 20 min and then filtered through a 0.22 μm membrane (Millipore) to remove cell debris, platelets and large vesicles.

4.16 | Statistical analysis

Origin and Image J software were used for all calculations. The linear fitting of different methods (Figure 4i) was performed to calculate the detection limits using Origin. The fluorescence intensity of images was calculated by Image J. Statistical differences were tested using one-sample *t*-test and one-way ANOVA with Bonferroni's post-hoc-test. Differences with $p < 0.05$ were considered to be statistically significantly different. ROC curves and AUC values were used to evaluate the specificity and sensitivity, while cut-off values reflected the point when the formula (specificity+sensitivity-1) reached the maximum value.

AUTHOR CONTRIBUTIONS

Jie He: Conceptualization; investigation; methodology; visualization; writing—original draft. **Hengyu Li**: Methodology; resources; supervision; writing—review and editing. **John Mai**: Visualization; writing—review and editing. **Yuqing Ke**: Formal analysis; methodology; visualization. **Chunhui Zhai**: Formal analysis; methodology; visualization. **Jiao Jiao Li**: Visualization; writing—review and editing. **Lai Jiang**: Data curation; resources. **Guangxia Shen**: Funding acquisition; project administration; resources; supervision; writing—review and editing. **Xianting Ding**: Conceptualization; funding acquisition; supervision; writing—review and editing

ACKNOWLEDGEMENTS

This work was supported by National Key R&D Program of China (2022YFC2601700, 2022YFF0710202) and NSFC Projects (32071405, 31771088, T2122002, 22077079, 81871448), Shanghai Municipal Science and Technology Project(22Z510202478), Shanghai Municipal Education Commission Project(21SG10), Shanghai Jiao Tong University Projects (YG2021ZD19, YG2022QN014, YG2023ZD09, Agri-X20200101, 2020 SJTU-HUJI), Shanghai Municipal Health Commission Project (2019CXJQ03). Thanks for AEMD SJTU, Shanghai Jiao Tong University Laboratory Animal Center for the supporting.

CONFLICT OF INTEREST STATEMENT

The authors declare no competing interests.

ASSOCIATED CONTENT

Fluorescence intensity analysis, SDS-PAGE of the probes, sequences of nucleic acids and experimental details are shown in **Supporting Information**. This material is available free of charge via the Internet.

DATA AVAILABILITY STATEMENT

The data that support the findings of this study are available from the corresponding author upon reasonable request.

ORCID

Xianting Ding https://orcid.org/0000-0002-1549-3499

REFERENCES

Chen, J. S., Ma, E., Harrington, L. B., Da Costa, M., Tian, X., Palefsky, J. M., & Doudna, J. A. (2018). CRISPR-Cas12a target binding unleashes indiscriminate single-stranded DNase activity. *Science*, *360*(6387), 436–439.

Chen, Y., Xue, F., Russo, A., & Wan, Y. (2021). Proteomic analysis of extracellular vesicles derived from MDA-MB-231 cells in microgravity. *The Protein Journal*, *40*(1), 108–118.

Chen, Y., Zhu, Q., Cheng, L., Wang, Y., Li, M., Yang, Q., Hu, L., Lou, D., Li, J., Dong, X., Lee, L. P., & Liu, F. (2021). Exosome detection via the ultrafast-isolation system: EXODUS. *Nature Methods*, *18*(2), 212–218.

Guo, Y., Tao, J., Li, Y., Feng, Y., Ju, H., Wang, Z., & Ding, L. (2020). Quantitative localized analysis reveals distinct exosomal protein-specific glycosignatures: Implications in cancer cell subtyping, exosome biogenesis, and function. *Journal of the American Chemical Society*, *142*(16), 7404–7412.

He, F., Liu, H., Guo, X., Yin, B. C., & Ye, B. C. (2017). Direct exosome quantification via bivalent-cholesterol-labeled DNA anchor for signal amplification. *Analytical Chemistry*, *89*(23), 12968–12975.

He, L., Yu, X., Huang, R., Jin, L., Liu, Y., Deng, Y., Li, S., Chen, H., Chen, Z., Li, Z., Xiao, P., & He, N. (2022). A novel specific and ultrasensitive method detecting extracellular vesicles secreted from lung cancer by padlock probe-based exponential rolling circle amplification. *Nano Today*, *42*, 101334.

Im, H., Shao, H., Park, Y. I., Peterson, V. M., Castro, C. M., Weissleder, R., & Lee, H. (2014). Label-free detection and molecular profiling of exosomes with a nano-plasmonic sensor. *Nature Biotechnology*, *32*(5), 490–495.

Ke, Y., Ghalandari, B., Huang, S., Li, S., Huang, C., Zhi, X., Cui, D., & Ding, X. (2022). 2'-O-Methyl modified guide RNA promotes the single nucleotide polymorphism (SNP) discrimination ability of CRISPR-Cas12a systems. *Chemical Science*, *13*(7), 2050–2061.

Kilic, T., Cho, Y. K., Jeong, N., Shin, I.-S., Carter, B. S., Balaj, L., Weissleder, R., & Lee, H. (2022). Multielectrode spectroscopy enables rapid and sensitive molecular profiling of extracellular vesicles. *ACS Central Science*, *8*(1), 110–117.

Kishi, J. Y., Lapan, S. W., Beliveau, B. J., West, E. R., Zhu, A., Sasaki, H. M., Saka, S. K., Wang, Y., Cepko, C. L., & Yin, P. (2019). SABER amplifies FISH: Enhanced multiplexed imaging of RNA and DNA in cells and tissues. *Nature Methods*, *16*(6), 533–544.

Kishi, J. Y., Schaus, T. E., Gopalkrishnan, N., Xuan, F., & Yin, P. (2018). Programmable autonomous synthesis of single-stranded DNA. *Nature Chemistry*, *10*(2), 155–164.

Kumar, P., Boyne, C., Brown, S., Qureshi, A., Thorpe, P., Synowsky, S. A., Shirran, S., & Powis, S. J. (2022). Tumour-associated antigenic peptides are present in the HLA class I ligandome of cancer cell line derived extracellular vesicles. *Immunology*, *166*(2), 249–264.

Li, S., Zhu, Y., Haghniaz, R., Kawakita, S., Guan, S., Chen, J., Li, Z., Mandal, K., Bahari, J., Shah, S., Guo, J., Kang, H., Sun, W., Kim, H.-J., Jucaud, V., Dokmeci, M. R., Kollbaum, P., Lee, C. H., & Khademhosseini, A. (2022). A microchambers containing contact lens for the noninvasive detection of tear exosomes. *Advanced Functional Materials*, *32*(44), 2206620.

Liang, K., Liu, F., Fan, J., Sun, D., Liu, C., Lyon, C. J., Bernard, D. W., Li, Y., Yokoi, K., Katz, M. H., Koay, E. J., Zhao, Z., & Hu, Y. (2017). Nanoplasmonic quantification of tumor-derived extracellular vesicles in plasma microsamples for diagnosis and treatment monitoring. *Nature Biomedical Engineering*, *1*(4), 0021.

Liu, C., Zhao, J., Tian, F., Cai, L., Zhang, W., Feng, Q., Chang, J., Wan, F., Yang, Y., Dai, B., Cong, Y., Ding, B., Sun, J., & Tan, W. (2019). Low-cost thermophoretic profiling of extracellular-vesicle surface proteins for the early detection and classification of cancers. *Nature Biomedical Engineering*, *3*(3), 183–193.

Mathieu, M., Martin-Jaular, L., Lavieu, G., & Thery, C. (2019). Specificities of secretion and uptake of exosomes and other extracellular vesicles for cell-to-cell communication. *Nature Cell Biology*, *21*(1), 9–17.

Melo, S. A., Luecke, L. B., Kahlert, C., Fernandez, A. F., Gammon, S. T., Kaye, J., LeBleu, V. S., Mittendorf, E. A., Weitz, J., Rahbari, N., Reissfelder, C., Pilarsky, C., Fraga, M. F., Piwnica-Worms, D., & Kalluri, R. (2015). Glypican-1 identifies cancer exosomes and detects early pancreatic cancer. *Nature*, *523*(7559), 177–82.

Merchant, M. L., Rood, I. M., Deegens, J. K. J., & Klein, J. B. (2017). Isolation and characterization of urinary extracellular vesicles: implications for biomarker discovery. *Nature Reviews Nephrology*, *13*(12), 731–749.

Mori, K., Hirase, M., Morishige, T., Takano, E., Sunayama, H., Kitayama, Y., Inubushi, S., Sasaki, R., Yashiro, M., & Takeuchi, T. (2019). A pretreatment-free, polymer-based platform prepared by molecular imprinting and post-imprinting modifications for sensing intact exosomes. *Angewandte Chemie-International Edition*, *58*(6), 1612–1615.

Pan, W.-L., Feng, J.-J., Luo, T.-T., Tan, Y., Situ, B., Nieuwland, R., Guo, J.-Y., Liu, C.-C., Zhang, H., Chen, J., Zhang, W.-H., Chen, J., Chen, X.-H., Chen, H.-Y., Zheng, L., Chen, J.-X., & Li, B. (2022). Rapid and efficient isolation platform for plasma extracellular vesicles: EV-FISHER. *Journal of Extracellular Vesicles*, *11*(11), e12281.

Park, J., Park, J. S., Huang, C.-H., Jo, A., Cook, K., Wang, R., Lin, H.-Y., Van Deun, J., Li, H., Min, J., Wang, L., Yoon, G., Carter, B. S., Balaj, L., Choi, G.-S., Castro, C. M., Weissleder, R., & Lee, H. (2021). An integrated magneto-electrochemical device for the rapid profiling of tumour extracellular vesicles from blood plasma. *Nature Biomedical Engineering*, *5*(7), 678–689.

Piao, Y. J., Kim, H. S., Hwang, E. H., Woo, J., Zhang, M., & Moon, W. K. (2018). Breast cancer cell-derived exosomes and macrophage polarization are associated with lymph node metastasis. *Oncotarget*, *9*(7), 7398–7410.

Qian, F., Huang, Z., Zhong, H., Lei, Q., Ai, Y., Xie, Z., Zhang, T., Jiang, B., Zhu, W., Sheng, Y., Hu, J., & Brinker, C. J. (2022). Analysis and biomedical applications of functional cargo in extracellular vesicles. *ACS Nano*, *16*(12), 19980–20001.

Qingqing, Z., Ruigong, S., Jian-Ping, W., & Qi, Z. (2016). Influence of magnetic Fe3O4 nanoparticles on fluorescence quenching of dye molecules. *Journal of Nanoscience and Nanotechnology*, *16*, 7432.

Rothlisberger, P., & Hollenstein, M. (2018). Aptamer chemistry. *Advanced Drug Delivery Reviews*, *134*, 3–21.

Shao, H., Im, H., Castro, C. M., Breakefield, X., Weissleder, R., & Lee, H. (2018). New technologies for analysis of extracellular vesicles. *Chemical Reviews*, *118*(4), 1917–1950.

Swarts, D. C., & Jinek, M. (2019). Mechanistic Insights into the cis- and trans-acting DNase activities of Cas12a. *Molecular Cell*, *73*(3), 589–600e4.

van Niel, G., Carter, D. R. F., Clayton, A., Lambert, D. W., Raposo, G., & Vader, P. (2022). Challenges and directions in studying cell-cell communication by extracellular vesicles. *Nature Reviews Molecular Cell Biology*, *23*(5), 369–382.

van Niel, G., D'Angelo, G., & Raposo, G. (2018). Shedding light on the cell biology of extracellular vesicles. *Nature Reviews Molecular Cell Biology*, *19*(4), 213–228.

Wan, Y., Cheng, G., Liu, X., Hao, S.-J., Nisic, M., Zhu, C.-D., Xia, Y.-Q., Li, W.-Q., Wang, Z.-G., Zhang, W.-L., Rice, S. J., Sebastian, A., Albert, I., Belani, C. P., & Zheng, S.-Y. (2017). Rapid magnetic isolation of extracellular vesicles via lipid-based nanoprobes. *Nature Biomedical Engineering*, *1*(4), 0058.

Wang, J., Wuethrich, A., Sina, A. A., Lane, R. E., Lin, L. L., Wang, Y., Cebon, J., Behren, A., & Trau, M. (2020). Tracking extracellular vesicle phenotypic changes enables treatment monitoring in melanoma. *Science Advances*, *6*(9), eaax3223.

Wang, S., Zhang, L., Wan, S., Cansiz, S., Cui, C., Liu, Y., Cai, R., Hong, C., Teng, I. T., Shi, M., Wu, Y., Dong, Y., & Tan, W. (2017). Aptasensor with expanded nucleotide using DNA nanotetrahedra for electrochemical detection of cancerous exosomes. *ACS Nano*, *11*(4), 3943–3949.

Witwer, K. W., Buzás, E. I., Bemis, L. T., Bora, A., Lässer, C., Lötvall, J., Nolte-'t Hoen, E. N., Piper, M. G., Sivaraman, S., Skog, J., Théry, C., Wauben, M. H., & Hochberg, F. (2013). Standardization of sample collection, isolation and analysis methods in extracellular vesicle research. *Journal of Extracellular Vesicles*, *2*(1), 20360.

Xu, R., Rai, A., Chen, M., Suwakulsiri, W., Greening, D. W., & Simpson, R. J. (2018). Extracellular vesicles in cancer — implications for future improvements in cancer care. *Nature Reviews Clinical Oncology*, *15*(10), 617–638.

Yan, S., Ahmad, K. Z., Li, S., Warden, A. R., Su, J., Zhang, Y., Yu, Y., Zhi, X., & Ding, X. (2021). Pre-coated interface proximity extension reaction assay enables trace protein detection with single-digit accuracy. *Biosensors & Bioelectronics*, *183*, 113211.

Yildizhan, Y., Vajrala, V. S., Geeurickx, E., Declerck, C., Duskunovic, N., De Sutter, D., Noppen, S., Delport, F., Schols, D., Swinnen, J. V., Eyckerman, S., Hendrix, A., Lammertyn, J., & Spasic, D. (2021). FO-SPR biosensor calibrated with recombinant extracellular vesicles enables specific and sensitive detection directly in complex matrices. *Journal of Extracellular Vesicles*, *10*(4), e12059.

Yu, D., Li, Y., Wang, M., Gu, J., Xu, W., Cai, H., Fang, X., & Zhang, X. (2022). Exosomes as a new frontier of cancer liquid biopsy. *Molecular Cancer*, *21*(1), 56.

Zhang, B., Ma, W., Li, F., Gao, W., Zhao, Q., Peng, W., Piao, J., Wu, X., Wang, H., Gong, X., & Chang, J. (2017). Fluorescence quenching-based signal amplification on immunochromatography test strips for dual-mode sensing of two biomarkers of breast cancer. *Nanoscale*, *9*(47), 18711–18722.

SUPPORTING INFORMATION

Additional supporting information can be found online in the Supporting Information section at the end of this article.

How to cite this article: He, J., Li, H., Mai, J., Ke, Y., Zhai, C., Li, J. J., Jiang, L., Shen, G., & Ding, X. (2023). Profiling extracellular vesicle surface proteins with 10 μL peripheral plasma within 4 h. *Journal of Extracellular Vesicles*, *12,* e12364. https://doi.org/10.1002/jev2.12364